IOP Publishing Journal of Physics D: Applied Physics
J. Phys. D: Appl. Phys. **40** (2007) 4793–4809 doi:10.1088/0022-3727/40/16/009

$O_2(^1\Delta)$ production and gain in plasma pumped oxygen–iodine lasers: consequences of NO and NO_2 additives

Ramesh A Arakoni[1], Natalia Y Babaeva[2] and Mark J Kushner[2,3]

[1] University of Illinois, Department of Aerospace Engineering, Urbana, IL 61801, USA
[2] Iowa State University, Department of Electrical and Computer Engineering, Ames, IA, 50011, USA

E-mail: arakoni@uiuc.edu, natalie5@iastate.edu and mjk@iastate.edu

Received 27 May 2007, in final form 29 May 2007
Published 3 August 2007
Online at stacks.iop.org/JPhysD/40/4793

Abstract
The 1.315 μm [$I(^2P_{1/2}) \rightarrow I(^2P_{3/2})$] transition of atomic iodine in the chemical oxygen–iodine laser (COIL) is pumped by sequential reactions of I_2 and I with $O_2(^1\Delta)$. In electrically pumped systems (eCOILs), electron impact excitation of O_2 produces the $O_2(^1\Delta)$ and also produces O atoms through dissociative excitation. The O atoms, through reactions with I_2, $I(^2P_{1/2})$ and $I(^2P_{3/2})$, lead to dissociation of I_2, quenching of the upper laser level and removal of the lower laser level. While dissociating I_2 is potentially beneficial, quenching of the upper laser level is detrimental and so management of the O atom density is necessary to maximize laser gain. In this regard, NO and NO_2 additives have been used to manage the O atom density by cyclically reacting with O and I. In this paper, results from a computational investigation of eCOIL systems using plug flow and two-dimensional models are discussed where NO and NO_2 additives are used. The system is a flowing plasma sustained in $He/O_2/NO$ mixtures with downstream injection of NO_2 followed by injection of I_2. We found that addition of NO and NO_2 is effective in managing the density of O atoms and maximizing gain by minimizing quenching of the upper laser level. We found that by optimizing the additives, laser gain can be maximized even though $O_2(^1\Delta)$ densities may be lower due to the management of quenching and dissociation reactions.

1. Introduction

Chemical oxygen–iodine lasers (COIL) operating on the 1.315 μm [$I(^2P_{1/2}) \rightarrow I(^2P_{3/2})$] transition of atomic iodine are being investigated due to their high efficiency and potential for multi-kilowatt CW operation [1–3]. A series of collisional transfer reactions between $O_2(^1\Delta)$, I_2 and ground state $I(^2P_{3/2})$ (to be referred to as I) result in excitation of the upper laser level $I(^2P_{1/2})$ (to be referred to as I^*). Typically $O_2(^1\Delta)$ is generated upstream of the laser cavity. I_2 is injected immediately prior to the cavity upon which the flow is supersonically expanded to lower the gas temperature as required to maximize the gain. In conventional COILs liquid-phase chemistries (reactions between basic H_2O_2 and Cl_2) produce the $O_2(^1\Delta)$ with high yields [4], although the use of liquid peroxides and Cl_2 gas to produce the $O_2(^1\Delta)$ creates challenges for storage and transport. Recently, efforts have focused on generating the $O_2(^1\Delta)$ in electrical discharges (eCOILs) due to the increased robustness and safety of the all gas-phase system [1–10]. Laser gain and oscillation have been demonstrated in eCOILs by Hicks *et al* [1] and Verdeyen *et al* [3].

A challenge in eCOILs is to produce sufficiently high yields of $O_2(^1\Delta)$, and hence laser gain, to enable the laser transition to be saturated and produce high power [5]. In

[3] Author to whom any correspondence should be addressed.

this regard, recent research has focused on tailoring the discharge parameters [6, 7, 10] and using additives such as CO, H_2, D_2 [8] and NO [9] to improve the excitation efficiency of $O_2(^1\Delta)$. NO and NO_2 are also used as additives to control the post-discharge chemistry [9]. In fact, all demonstrations of laser gain and oscillation to date have used flowing plasmas in He/O_2 mixtures with NO as an additive.

eCOILs differ from conventional COILs in that atomic oxygen is also produced in the electric discharge by electron impact dissociation of O_2. The O atoms flow downstream where 3-body reactions produce O_3 and the remaining O atoms may react with the injected I_2. Beneficial reactions of O with I_2 produce I atoms, thereby eliminating the expense of $O_2(^1\Delta)$ molecules for initiating the dissociating reactions. Detrimental reactions involving O atoms include quenching of I^* by O which reduces gain. As such, management of the O atom density is important to optimize these opposing effects.

Injection of NO or NO_2 through or downstream of the discharge in eCOIL systems has two goals; improving the efficiency of direct production of $O_2(^1\Delta)$ in the discharge by electron impact and management of the O atom density downstream of the plasma. Including NO in the gas stream flowing through the discharge has, in part, the goal of improving production of $O_2(^1\Delta)$. NO, having a lower ionization potential (9.26 eV) than either O_2 or He, is likely to provide more rapid ionization with the possibility of lowering the operating E/N (electric field/gas number density) and electron temperature, T_e. Lowering T_e from the values typical of self-sustained He/O_2 mixtures is advantageous in more efficiently producing $O_2(^1\Delta)$ by direct electron impact [6, 8, 11]. Discharges in NO have also been known to produce $O_2(^1\Delta)$ in relatively large amounts even though O_2 may not be present as a feedstock gas [12]. However, when flowing NO through the discharge, some of the power that would otherwise be available to excite O_2 is dissipated by excitation and ionization of NO, an unwanted consequence.

In addition to possibly improving the production of $O_2(^1\Delta)$, NO and NO_2 are potentially effective in managing the inventory of O atoms through direct and cyclic reactions which have the effect of converting O atoms back into O_2. In the context of eCOIL systems where I_2 is injected, O atoms are beneficial by dissociating I_2 (and product species IO) to form I atoms which are then pumped to I^* by collisions with $O_2(^1\Delta)$. The O atoms are detrimental by quenching I^*. Totally eliminating O atoms is therefore not necessarily beneficial. NO and NO_2 also have secondary effects in that they react with I atoms forming intermediary species such as INO, and INO_2 which further react with I to reform I_2 [13].

In this paper, we report on results from a computational investigation of the consequences of NO and NO_2 additives on flowing He/O_2 plasmas and their afterglows with I_2 injection in the context of eCOIL systems. These investigations were conducted using plug flow and 2-dimensional (2D) plasma-hydrodynamics models. Although for most conditions the addition of NO to the inlet gas stream reduced the density of $O_2(^1\Delta)$, it ultimately increased the densities of I^* downstream of the discharge through management of the O atom density. The inlet NO mole fraction also typically increased the extent of the region over which positive laser gain could be achieved. This can be particularly useful in high speed flows where mixing lengths are longer. Injection of NO_2 in the post-discharge flow can help in rapidly scavenging O atoms in two body reactions (as compared with scavenging by NO which proceeds by a 3-body mechanism). In general, addition of NO_2 in the post-discharge region improves laser gain [9]. The downside to NO_2 injection is a rise in gas temperature due to the exothermicity of the reactions between NO_2 and O.

The models used in this investigation are described in section 2 followed by a discussion of the reaction mechanism in sections 3. In section 4 the consequences of NO flowing through the discharge and its influence on downstream kinetics when I_2 is injected are described. In section 5, the post-discharge kinetics with NO_2 addition upstream of I_2 injection are discussed. Our concluding remarks are in section 6.

2. Description of models

This investigation was conducted using a plug flow model, *GlobalKIN*, and a 2D plasma hydrodynamics model, *nonPDPSIM*. *GlobalKIN* has been previously described in [11, 14] and so will only be briefly discussed here. *GlobalKIN* consists of a volume averaged plasma chemistry module and an electron energy transport module. The plasma chemistry module provides the time rate of change of species densities based on gas-phase chemistry and surface reactions. Electron temperature, T_e, and average gas temperature, T_g, are also solved for by integrating their respective conservation equations. The electron energy transport module consists of a solution of Boltzmann's equation for the electron energy distribution (EED) which provides electron impact rate coefficients based on the EEDs and fundamental cross-sections.

For plasmas flowing through cylinders having large aspect ratios, transport to the radial surfaces is taken into account by using a diffusion length. By simultaneously calculating the axial speed of the flow based on constant pressure, change in enthalpy, species densities, conservation of mass and gas temperature, the integration in time is mapped to axial position. The resulting rate equations are integrated in time using a stiff ordinary differential equation solver. To address the use of additives, *GlobalKIN* was modified to enable the downstream injection of gases into the flow. Injection nozzles were treated as point sources of mass, axial momentum and enthalpy. Power deposition as a function of axial position must be specified in *GlobalKIN*. This distribution was estimated by averaging the power deposition obtained from the *nonPDPSIM* over the cross-section of the tube.

nonPDPSIM has been discussed in detail in [15, 16], and so will only be briefly described here along with pertinent updates to the model. Continuity equations for charged gas-phase species, surface charges and Poisson's equation for the electric potential are simultaneously implicitly integrated in time. Updates of these quantities are followed, in a time splicing manner, with updates of T_e and neutral species densities using a modified form of the compressible Navier–Stokes equations for continuity, momentum and energy (gas temperature) which accounts for interactions with the plasma. A circuit model was

used to interface the plasma with metal surfaces connected to a voltage source and circuit elements (e.g. ballast resistor). The power supply voltage was adjusted to deposit the specified power in the plasma.

To address the longer time scales for the injection and mixing of additives downstream the following method was used. It was determined and validated that the injected gases were sufficiently far downstream from the plasma that their presence did not affect the plasma properties. As such, plasma quantities (for example, electron density (n_e), T_e, rates of electron impact reactions, and ionization sources) were calculated until a quasi-steady state was reached after which these quantities were 'frozen' in the upstream plasma zone. Following the establishment of the plasma properties only the neutral fluid equations were integrated (accounting for injection of gases downstream) which did not affect quantities upstream in the plasma. This enabled a longer time-step downstream where the injection kinetics occurred.

3. Reaction mechanism

The species included in the reaction mechanism are e, He, $He(^2S)$, He^+, O_2, $O_2(v)$, $O_2(^1\Delta)$, $O_2(^1\Sigma)$, O_2^-, O_2^+, O, $O(^1D)$, $O(^1S)$, O^-, O^+, O_3, O_3^-, NO, NO^+, NO_2, NO^-, NO_2^-, N, N_2, I_2, I_2^*, $I(^2P_{3/2})$, $I(^2P_{1/2})$, IO, INO and INO_2. $He(^2P)$ was included for purposes of electron energy loss in solving Boltzmann's equation but was lumped with $He(^2S)$ in the chemical kinetics. $O_2(v)$ represents the sum of the first four vibrational levels of O_2. The vibrational levels of N_2 were not included as individual species in the reaction mechanism as N_2 densities were small and predominantly produced downstream of the discharge where electron impact processes are negligible. Excitation of the first five vibrational levels of NO ($\Delta\varepsilon$ = 0.23, 0.46, 0.69, 0.91 and 1.13) and the electronic states $NO(a^2\Sigma)$ ($\Delta\varepsilon$ = 5.48 eV), $NO(c^2\Pi)$ ($\Delta\varepsilon$ = 6.5 eV) and $NO(b^4\Sigma)$ ($\Delta\varepsilon$ = 7.58 eV) were included for purposes of energy loss collisions with ground state NO. The densities of these states were not explicitly tracked in the model. The negative ions NO^- and NO_2^- were included only in *GlobalKIN* after confirming that their exclusion does not make a significant change to the reaction kinetics in *nonPDPSIM*. Their exclusion from *nonPDPSIM* was for the purpose of speeding the calculation.

The reaction mechanism builds upon that previously developed for He/O_2 discharges and which is discussed in [14]. The processes that were added to that reaction mechanism to account for the injection of NO, NO_2 and I_2 are listed in table 1.

The majority of $O_2(^1\Delta)$ is produced by electron impact excitation of ground state O_2 in the plasma zone, and secondarily by excitation of $O_2(^1\Sigma)$ followed by quenching to $O_2(^1\Delta)$ by collisions with O atoms,

$$e + O_2 \rightarrow O_2(^1\Delta) + e, \quad (1)$$

$$e + O_2 \rightarrow O_2(^1\Sigma) + e, \quad (2)$$

$$O + O_2(^1\Sigma) \rightarrow O_2(^1\Delta) + O, \quad (3)$$

$$e + O_2 \rightarrow O + O + e, \quad (4)$$

$$e + O_2 \rightarrow O(^1D) + O + e. \quad (5)$$

Electron impact dissociation of O_2 (equations (4) and (5)) is a significant source of O atoms and, in part, the motivation for injection of NO and NO_2 to manage the resulting flow of O atoms. For self-sustaining discharges, roughly one O atom is generated for every $O_2(^1\Delta)$ produced in the plasma zone. By lowering T_e to 1–1.5 eV from self-sustaining values of 2–3 eV by, for example, using the spiker–sustainer methods, the rate of excitation of $O_2(^1\Delta)$ can be increased relative to electron impact dissociation [11].

The negative ion chemistry of He/O_2 mixtures is initiated by dissociative attachment and 3-body reactions,

$$e + O_2 \rightarrow O^- + O, \quad (6)$$

$$e + O_2 + M \rightarrow O_2^- + M, \ (k = 3.6 \times 10^{-31} T_e^{-0.5}\ cm^6\ s^{-1}), \quad (7)$$

where M is a third body and k is the rate coefficient. O_2^- subsequently charge exchanges with O atoms to form O^- or associatively detaches to form O_3. A similar process occurs with O^- to reform O_2,

$$O_2^- + O \rightarrow O_2 + O^-, \quad (k = 1.5 \times 10^{-10}\ cm^3\ s^{-1}), \quad (8)$$

$$O_2^- + O \rightarrow O_3 + e, \quad (k = 1.5 \times 10^{-10}\ cm^3\ s^{-1}), \quad (9)$$

$$O^- + O \rightarrow O_2 + e, \quad (k = 2 \times 10^{-10}\ cm^3\ s^{-1}). \quad (10)$$

Through dissociative detachment reactions, both O^- and O_2^- react with $O_2(^1\Delta)$ to form O_3, and to quench $O_2(^1\Delta)$,

$$O^- + O_2(^1\Delta) \rightarrow O_3 + e, \quad (k = 3 \times 10^{-10}\ cm^3\ s^{-1}), \quad (11)$$

$$O_2^- + O_2(^1\Delta) \rightarrow O_2 + O_2 + e, \quad (k = 2 \times 10^{-10}\ cm^3\ s^{-1}). \quad (12)$$

An important motivation for flowing NO through the plasma zone is that it has a smaller ionization potential than O_2 and He and so should produce more ionization at a lower T_e,

$$e + NO \rightarrow NO^+ + e + e, \quad (\Delta\varepsilon = 9.26\ eV). \quad (13)$$

This ionization does, however, come at the cost of channelling discharge power into NO (e.g. vibrational excitation and dissociation), power that might otherwise be deposited into O_2. This power therefore does not directly lead to generation of $O_2(^1\Delta)$. Since NO^+ has the smallest ionization potential among all the atoms and molecules in this mechanism, significant amounts of NO^+ are formed by charge-exchange reactions with He^+, O^+ and O_2^+. Dissociative recombination of NO^+ with electrons can produce N, O and $O(^1D)$, as well as contribute to gas heating through Frank–Condon processes,

$$e + NO^+ \rightarrow N + O, \quad (k = 3.4 \times 10^{-7} T_e^{-0.5}\ cm^3\ s^{-1}, \ \Delta H = -2.77\ eV), \quad (14)$$

$$\rightarrow N + O(^1D) \quad (k = 6.0 \times 10^{-8} T_e^{-0.5}\ cm^3\ s^{-1}, \ \Delta H = -0.8\ eV), \quad (15)$$

where ΔH is the change in enthalpy of the recombination event.

NO also intercepts the negative ion chemistry through charge-exchange reactions and associative attachment,

$$O^- + NO \rightarrow NO_2 + e, \quad (k = 2.8 \times 10^{-10}\ cm^3\ s^{-1}), \quad (16)$$

$$O^- + NO_2 \rightarrow NO_2^- + O, \quad (k = 1.2 \times 10^{-9}\ cm^3\ s^{-1}). \quad (17)$$

These reactions are potentially beneficial in two ways. They increase the electron density which can lower T_e into a more favourable range for exciting $O_2(^1\Delta)$ and they reduce the density of O^- which would otherwise quench $O_2(^1\Delta)$ to form

Table 1. Processes added to He/O_2 reaction mechanism with NO, NO_2 and I_2.

Species		
He	NO	e
He^*	NO_2	He^+
O	N	O_2^+
$O(^1D)$	N_2	O_2^-
$O(^1S)$	I_2	O^+
O_2	I	O^-
$O_2(v)$	I^*	O_3^-
$O_2(^1\Delta)$	IO	NO^+
$O_2(^1\Sigma)$	INO	NO^-
O_3	INO_2	NO_2^-

Reaction	Rate coefficient[a]	Reference
$e + NO \rightarrow N + O^-$	[b]	[18]
$e + NO \rightarrow N + O + e$	[b]	[19]
$e + NO \rightarrow NO^+ + e + e$	[b]	[20]
$e + NO \rightarrow N + O^+ + e + e$	[b]	[20]
$e + NO^+ \rightarrow N + O$	$3.4 \times 10^{-7}\ T_e^{-0.5}$	[21]
$e + NO^+ \rightarrow N + O(^1D)$	$6.0 \times 10^{-7}\ T_e^{-0.5}$	[21]
$e + NO + He \rightarrow NO^- + He$	$1.0 \times 10^{-32}\ T_e^{-0.5}$	[22]
$e + NO + NO \rightarrow NO^- + NO$	$6.5 \times 10^{-31}\ T_e^{-0.5}$	[22]
$He^* + NO \rightarrow He + NO^+ + e$	2.5×10^{-10}	[c]
$He^+ + NO \rightarrow He + NO^+$	1.6×10^{-9}	[23]
$He^+ + NO \rightarrow He + N + O^+$	4.2×10^{-10}	[23]
$O^+ + NO \rightarrow O + NO^+$	1.7×10^{-12}	[23]
$O_2^+ + NO \rightarrow O_2 + NO^+$	4.5×10^{-10}	[23]
$O_2^+ + N \rightarrow NO^+ + O$	1.2×10^{-10}	[23]
$NO^-, NO_2^- + M^+ \rightarrow NO, NO_2 + M$[d]	$2.0 \times 10^{-7}\ (T_g/300)^{-1}$	[c]
$NO^+ + M^- \rightarrow NO + M$[e]	$2.0 \times 10^{-7}\ (T_g/300)^{-1}$	[c]
$O^- + NO \rightarrow NO_2 + e$	$2.8 \times 10^{-10}\ (T_g/300)^{0.5}$	[23]
$O^- + N \rightarrow NO + e$	$2.2 \times 10^{-10}\ (T_g/300)^{0.5}$	[23]
$O^- + NO_2 \rightarrow NO_2^- + e$	$1.2 \times 10^{-9}\ (T_g/300)^{0.5}$	[23]
$O_2^- + N \rightarrow NO_2 + e$	$4.0 \times 10^{-10}\ (T_g/300)^{0.5}$	[23]
$O_2^- + NO_2 \rightarrow NO_2^- + O_2$	$7.0 \times 10^{-10}\ (T_g/300)^{0.5}$	[23]
$O_3^- + NO \rightarrow NO_2^- + O_2$	$2.2 \times 10^{-12}\ (T_g/300)^{0.5}$	[23]
$NO^- + NO \rightarrow NO + NO + e$	$5.0 \times 10^{-12}\ (T_g/300)^{0.5}$	[23]
$NO^- + He \rightarrow NO + He + e$	$2.4 \times 10^{-13}\ (T_g/300)^{0.5}$	[23]
$NO^- + NO_2 \rightarrow NO + NO_2^-$	$7.4 \times 10^{-10}\ (T_g/300)^{0.5}$	[23]
$NO^- + O_2 \rightarrow NO + O_2^-$	$5.0 \times 10^{-10}\ (T_g/300)^{0.5}$	[23]
$NO_2^- + O_3 \rightarrow O_3^- + NO_2$	$9.4 \times 10^{-12}\ (T_g/300)^{0.5}$	[23]
$NO + O_3 \rightarrow NO_2 + O_2$	$1.4 \times 10^{-12}\ e^{-1310/T_g}$	[24]
$NO + O_2(^1\Delta) \rightarrow NO + O_2$	3.5×10^{-17}	[25]
$NO + O(^1D) \rightarrow N + O_2$	5.0×10^{-15}	[26]
$NO + O(^1D) \rightarrow NO + O$	4.0×10^{-11}	[27]
$NO + O + M \rightarrow NO_2 + M$[f]	$1.0 \times 10^{-31}\ (T_g/300)^{-1.6}$	[24]
$NO_2 + O \rightarrow NO + O_2$	$4.2 \times 10^{-12}\ e^{273/T_g}$	[24]
$NO_2 + O(^1D) \rightarrow NO_2 + O$	3.2×10^{-10}	[28]
$NO_2 + O(^1D) \rightarrow NO + O_2$	3.0×10^{-10}	[28]
$N + O_2 \rightarrow NO + O$	$2.4 \times 10^{-11}\ e^{-5320/T_g}$	[29]
$N + NO_2 \rightarrow NO + NO$	6.1×10^{-12}	[30]
$N + NO_2 \rightarrow N_2 + O + O$	2.4×10^{-12}	[30]
$N + NO_2 \rightarrow N_2 + O_2$	1.8×10^{-12}	[30]
$N + O + M \rightarrow NO + M$[f]	$5.5 \times 10^{-33}\ e^{155/T_g}$	[31]
$O_2(^1\Delta) + O_2 + O \rightarrow O_2 + O_2 + O$	1.0×10^{-32}	[10]
$O_2(^1\Sigma) + I_2 \rightarrow O_2 + I + I$	2.8×10^{-11}	[9]
$O_2(^1\Sigma) + I_2 \rightarrow O_2(^1\Delta) + I_2$	2.3×10^{-11}	[9]
$O_2(^1\Sigma) + I_2 \rightarrow O_2 + I_2$	6.0×10^{-12}	[9]
$O_2(^1\Delta) + I_2 \rightarrow O_2 + I_2^*$	7.0×10^{-15}	[9]
$O_2(^1\Delta) + I_2 \rightarrow O_2 + I_2$	5.0×10^{-16}	[9]
$O + I_2 \rightarrow IO + I$	1.4×10^{-10}	[9]
$He + I_2^* \rightarrow He + I_2$	9.8×10^{-12}	[9]
$O_2 + I_2^* \rightarrow O_2 + I_2$	4.9×10^{-12}	[9]
$O_2(^1\Delta) + I_2^* \rightarrow O_2 + I + I$	3.0×10^{-10}	[9]
$O_2(^1\Delta) + I \rightarrow O_2 + I^*$	$7.7 \times 10^{-11}\ (T_g/300)^{-1.0}$	[9]
$O_2(^1\Delta) + I \rightarrow O_2 + I$	1.0×10^{-15}	[9]
$O_3 + I \rightarrow O_2 + IO$	$2.0 \times 10^{-11}\ e^{-890/T_g}$	[9]
$He + I^* \rightarrow He + I$	5.0×10^{-18}	[9]
$O_2(^1\Delta) + I^* \rightarrow O_2(^1\Sigma) + I$	$8.4 \times 10^{-15}\ (T_g/300)^{3.8}\ e^{700/T_g}$	[9]

Table 1. Continued.

Reaction	Rate coefficient[a]	Reference
$O_2(^1\Delta) + I^* \rightarrow O_2 + I$	1.10×10^{-13}	[9]
$O_2 + I^* \rightarrow O_2^* + I$	$1.0 \times 10^{-10}\ (T_g/300)^{-1.0}\ e^{-403/T_g}$	[9]
$O + I^* \rightarrow O + I$	8.0×10^{-12}	[9]
$NO + I^* \rightarrow NO + I$	1.2×10^{-13}	[9]
$NO_2 + I^* \rightarrow NO_2 + I$	8.5×10^{-14}	[9]
$I_2 + I^* \rightarrow I_2^* + I$	$1.40 \times 10^{-13}\ e^{1600/T_g}$	[9]
$IO + IO \rightarrow O_2 + I + I$	8.2×10^{-11}	[9]
$NO + IO \rightarrow NO_2 + I$	$4.3 \times 10^{-12}\ e^{-397/T_g}$	[32]
$O + IO \rightarrow O_2 + I$	1.4×10^{-10}	[9]
$O + IO \rightarrow O_2(^1\Delta) + I$	1.5×10^{-11}	[9]
$I + INO \rightarrow I_2 + NO$	1.6×10^{-10}	[13]
$I + INO_2 \rightarrow I_2 + NO_2$	8.3×10^{-11}	[13]
$INO + INO \rightarrow I_2 + NO + NO$	$8.4 \times 10^{-11}\ e^{-2620/T_g}$	[13]
$INO_2 + INO_2 \rightarrow I_2 + NO_2 + NO_2$	$2.9 \times 10^{-11}\ e^{-2600/T_g}$	[13]
$I + I + I_2 \rightarrow I_2 + I_2$	3.6×10^{-30}	[9]
$I + I + He \rightarrow I_2 + He$	3.8×10^{-33}	[9]
$I + I + O_2 \rightarrow I_2 + O_2$	3.3×10^{-32}	[9]
$I + I^* + I_2 \rightarrow I + I + I_2$	3.6×10^{-30}	[9]
$I + I + O_2 \rightarrow I_2 + O_2(^1\Delta)$	3.7×10^{-33}	[9]
$I + NO + He \rightarrow INO + He$	$6.0 \times 10^{-33}\ (T_g/300)^{-1.0}$	[13]
$I + NO + O_2 \rightarrow INO + O_2$	1.6×10^{-32}	[13]
$I + NO_2 + He \rightarrow INO_2 + He$	$1.5 \times 10^{-31}\ (T_g/300)^{-1.0}$	[13]
$I + NO_2 + O_2 \rightarrow INO_2 + O_2$	2.6×10^{-31}	[13]
$I^* \rightarrow I$	10	[33]

[a] Rate coefficient in $cm^3\ s^{-1}$ for 2-body reactions, and $cm^6\ s^{-1}$for 3-body reactions and s^{-1} for radiation reactions.
[b] Rate coefficients calculated using cross-section data from the indicated reference.
[c] Estimated.
[d] Where M is one of the cations O^+, O_2^+, He^+ or NO^+.
[e] Where M is one of the anions O^-, O_2^- or O_3^-.
[f] Where M is one of the major neutral species He, O_2, O_2(v), $O_2(^1\Delta)$, O or O_3.

O_3. The negative ions NO^- and NO_2^- were not included in the 2D model (to increase computational speed), whereas they were included in the plug flow model. Computational experiments were conducted using the plug flow model to quantify the effects of the NO^- and NO_2^- and are discussed below.

One of the primary motivations of injecting NO and NO_2 is in their potential for managing of the O atom inventory. Much of this chemistry is cyclic. NO reacts with O to form NO_2 which then further reacts with O to regenerate O_2,

$$NO + O + M \rightarrow NO_2 + M, \quad (k = 1.0 \times 10^{-31}(T_g/300)^{-1.6}, \quad \Delta H = -3.18\,eV), \tag{18}$$

$$NO_2 + O \rightarrow NO + O_2, \quad (k = 4.2 \times 10^{-12}\exp(273/T_g), \quad \Delta H = -2.0\,eV). \tag{19}$$

This is an important reaction chain that can reduce the inventory of O atoms and so eliminate a quencher of the upper laser level, I^*. At low pressures where the 3-body density is low, the rate of reaction of O with NO_2 occurs at a higher rate than with NO. Hence addition of NO_2 in the downstream region may be preferred over that of NO if the residence time in the flow tube is a limiting factor. These reactions are, however, exothermic and so can increase the gas temperature which is generally not beneficial.

Laser gain is ultimately achieved by injection of I_2 downstream of the plasma zone, and by its reacting with O, $O_2(^1\Delta)$, and $O_2(^1\Sigma)$ to create I atoms and to pump the upper laser level. In a conventional COIL there is a negligible inventory of O atoms and $O_2(^1\Sigma)$, and so the dissociation of I_2 is dominantly by $O_2(^1\Delta)$ in a two-step process,

$$O_2(^1\Delta) + I_2 \rightarrow O_2 + I_2^*, \quad (k = 7 \times 10^{-15}\,cm^3\,s^{-1}), \tag{20}$$

$$O_2(^1\Delta) + I_2^* \rightarrow O_2 + I + I, \quad (k = 3 \times 10^{-10}\,cm^3\,s^{-1}). \tag{21}$$

In eCOIL, the presence of $O_2(^1\Sigma)$ and O helps in dissociating I_2 and producing I atoms. A reaction intermediate IO is also helpful in this regard,

$$O_2(^1\Sigma) + I_2 \rightarrow O_2 + I + I, \quad (k = 2.8 \times 10^{-11}\,cm^3\,s^{-1}), \tag{22}$$

$$O + I_2 \rightarrow IO + I, \quad (k = 1.4 \times 10^{-10}\,cm^3\,s^{-1}), \tag{23}$$

$$O + IO \rightarrow I + O_2, \quad (k = 1.4 \times 10^{-10}\,cm^3\,s^{-1}). \tag{24}$$

The laser pumping reaction by $O_2(^1\Delta)$ in collisions with I is favoured at lower temperatures over its endothermic back reaction,

$$O_2(^1\Delta) + I \rightarrow O_2 + I^*, \quad (k = 7.7 \times 10^{-11}(T_g/300)^{-1}\,cm^3\,s^{-1}), \tag{25}$$

$$O_2 + I^* \rightarrow O_2(^1\Delta) + I, \quad (k = 1.0 \times 10^{-10}(T_g/300)^{-1}e^{-403/T_g}). \tag{26}$$

To suppress the back reaction, the laser cavity is typically placed in a supersonically expanded flow to lower the translational temperature. As such, the threshold yield, Y_{th}, of $O_2(^1\Delta)$ required for positive optical gain in an undissociated flow of O_2 is [17],

$$Y_{th} = \frac{[O_2(^1\Delta)]}{[O_2]} = \frac{1}{1 + 1.5\exp(401/T_g)}. \tag{27}$$

For example, in an undissociated flow of O_2, the threshold yield at room temperature is 15% whereas at 180 K the threshold yield is 6%.

Quenching of I^* occurs dominantly by reactions with O and O_2 (the backward reaction), and to a lesser extent with $O_2(^1\Delta)$ and NO,

$$O + I^* \rightarrow O + I, \quad (k = 8.0 \times 10^{-12}\,\mathrm{cm^3\,s^{-1}}), \tag{28}$$

$$NO + I^* \rightarrow NO + I, \quad (k = 1.2 \times 10^{-13}\,\mathrm{cm^3\,s^{-1}}). \tag{29}$$

NO and NO_2 also help in removing ground state I atoms and so aid in maintaining the inversion,

$$I + NO + O_2 \rightarrow INO + O_2, \quad (k = 1.6 \times 10^{-32}\,\mathrm{cm^6\,s^{-1}}), \tag{30}$$

$$I + NO + He \rightarrow INO + He, \quad (k = 6.0 \times 10^{-33}\,\mathrm{cm^6\,s^{-1}}), \tag{31}$$

$$I + NO_2 + O_2 \rightarrow INO_2 + O_2, \quad (k = 2.6 \times 10^{-31}\,\mathrm{cm^6\,s^{-1}}), \tag{32}$$

$$I + NO_2 + He \rightarrow INO_2 + He, \quad (k = 6.0 \times 10^{-33}\,\mathrm{cm^6\,s^{-1}}). \tag{33}$$

The INO_x species in turn abstract I atoms to release I_2 and NO_x back into the flow,

$$INO + I \rightarrow I_2 + NO, \quad (k = 1.6 \times 10^{-10}\,\mathrm{cm^3\,s^{-1}}), \tag{34}$$

$$INO_2 + I \rightarrow I_2 + NO_2, \quad (k = 8.3 \times 10^{-11}\,\mathrm{cm^3\,s^{-1}}). \tag{35}$$

Typically, the injection of I_2 occurs during or following a supersonic expansion of the gas to velocities equivalent to Mach 2 or Mach 3 to lower T_g to decrease the yields of $O_2(^1\Delta)$ required to achieve positive gain. Accurately simulating a supersonic expansion is difficult in our modelling platform. In order to provide a best case estimate for laser gain we used for the temperature of the reactions in equations (25) and (26) a value appropriate for a Mach 2 flow. This temperature can be approximated from

$$\frac{T_0}{T_g} = \left(1 + \frac{\gamma - 1}{2} M^2\right), \tag{36}$$

where T_0 is the stagnation (or tank) temperature, γ is the ratio of specific heats and M is the Mach number. For $M = 2$ and $T_0 = 300$ K, this ratio is ≈2.18, and would lead to a gas temperature of 137 K. The reaction mechanism was validated by comparing with experimental data from Carroll *et al* [34], as discussed below.

4. Consequences of NO in the inlet flow

A schematic of the cylindrically symmetric, 6 cm diameter flow tube used in this study is shown in figure 1. In the base case, a power of 40 W was capacitively coupled using ring electrodes operated at 25 MHz. A mixture of $He/O_2/NO$ at 3 Torr entered through the inlet at a flow rate of 6 slpm which corresponds to an axial speed of ≈890 cm s^{-1}. The flow consisted of 30% O_2 with the balance divided between He and NO. The NO mole fraction was varied from 0–10%. Two injection nozzles are located downstream. (In the 2D cylindrically symmetric geometry these nozzles appear to be rings.) The first nozzle at 51.5 cm was used to inject a mixture of $He/NO/NO_2$. The second nozzle at 64.5 cm injected a mixture of He/I_2. At the outlet, axial gradients were assumed to be zero and the exit speeds were adjusted to maintain constant pressure and mass flux.

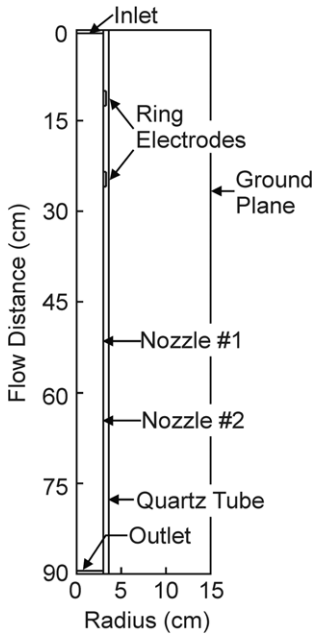

Figure 1. Geometry of the cylindrically symmetric reactor. The flow enters from the top and is pumped from the bottom. Discharge power at 25 MHz is capacitively coupled through ring electrodes. Two nozzles downstream of the discharge inject mixtures of He, NO, NO_2 and/or I_2.

Plasma characteristics (n_e, T_e, negative total negative ion density M^-, total positive ion density M^+ and power density) obtained with *nonPDPSIM* are shown in the vicinity of the electrodes in figure 2 for the base case having an inlet flow of $He/O_2/NO = 67/30/3$. T_e in the bulk of the discharge was 2.3 eV and the peak electron density was 9.0×10^9 cm^{-3}. Since NO and O_2 are attaching species, the negative ion density (maximum of 1.1×10^{10} cm^{-3}) is commensurate with n_e. The electron density is fairly symmetric between the electrodes and relatively uniform. The power deposition is moderately higher near the upstream electrode due to gas heating which reduces the neutral densities downstream. This is not a general result as higher power deposition and more rarefaction can produce regions of locally intense power deposition near the downstream electrode.

The densities of the neutral species O, $O_2(^1\Delta)$, I and I^* and T_g for the base case are shown in figure 3. A flow of 36 sccm of pure NO was injected through the first nozzle and a flow of 100 sccm of $He/I_2 = 99/1$ was injected through the second nozzle. Having few quenchers at these pressures, the $O_2(^1\Delta)$ accumulates as the gas flows through the discharge reaching a maximum value of 1.35×10^{15} cm^{-3}. The $O_2(^1\Delta)$ density remains nearly constant thereafter until the injection point for I_2. Reactions of $O_2(^1\Delta)$ with I_2 and I (the latter being the laser pumping reaction producing I^*) reduce its density by a factor of five to 2.7×10^{14} cm^{-3}.

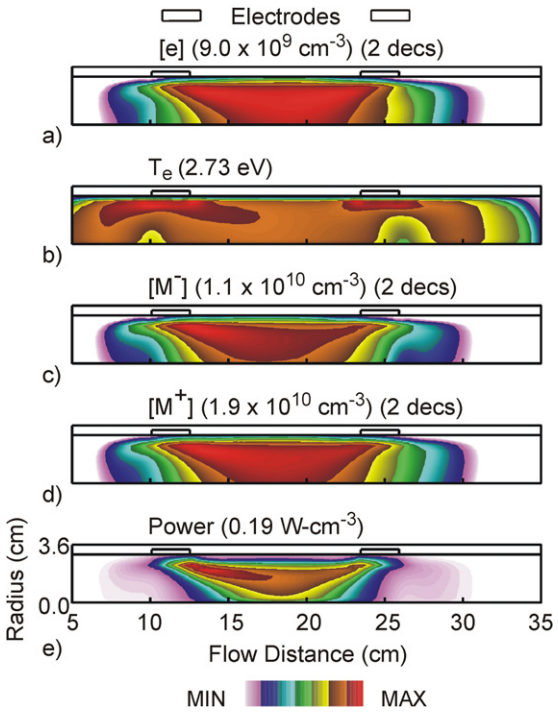

Figure 2. Base case plasma characteristics from the 2D model for 3 Torr, 40 W, He/O_2/NO = 67/30/3 and a flow rate of 6 slpm. (*a*) Electron density, (*b*) electron temperature, (*c*) sum of negative ion densities, (*d*) sum of positive ion densities and (*e*) power density. The scales are linear for T_e and power (0 to maximum), and the densities are plotted on a 2-decade log scale.

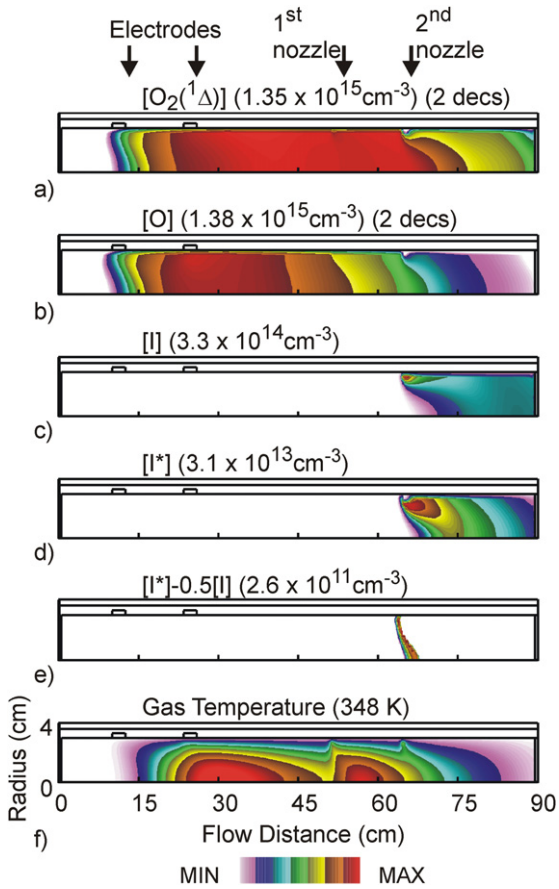

Figure 3. Neutral species densities and T_g for the base case. 36 sccm of pure NO was injected through the first nozzle and 100 sccm of He/I_2 = 99/1 was injected through the second nozzle. Densities of (*a*) $O_2(^1\Delta)$, (*b*) O, (*c*) I, (*d*) I*, (*e*) inversion density ([I*]-0.5[I]) and (*f*) gas temperature. The scales are linear except for $O_2(^1\Delta)$ and O which are plotted on a 2-decade log scale. Injection of NO decreases the flow of O and injection of I_2 consumes $O_2(^1\Delta)$. Exothermic reactions at both injection points produce local maxima in T_g.

Similar to $O_2(^1\Delta)$, the density of O atoms accumulate from electron impact dissociation of O_2 passing through the discharge (with a small amount of depletion of the O in forming O_3) until the injection point of NO at the first nozzle. The O densities decrease from a peak value of 1.4×10^{15} to 4.0×10^{14} cm^{-3} downstream of the NO injection due to its reaction with NO. The remaining O atoms flow to the injection point of I_2 where they are further depleted in dissociating reactions with I_2. The I_2 is nearly completely dissociated by reactions with the O atoms to form I. Pumping reactions between $O_2(^1\Delta)$ and I produce I*. The region of positive gain (where the inversion density $G = [I^*] - 1/2[I] > 0$) is a narrow band downstream of the I_2 injection point, with a peak value of $G = 2.6 \times 10^{11}$ cm^{-3}.

T_g has two local maxima. The first is due to discharge Joule heating, Frank–Condon heating and exothermic reactions of NO with O reaching 340 K adjacent to the downstream electrode. As the walls are held at 300 K, the gas rapidly cools by thermal conduction. A second local maximum occurs downstream of the first injection nozzle (up to 348 K) due to additional exothermic reactions of O and the newly injected NO.

To investigate the consequences of NO in the inlet flow over a wider parameter space, the plug flow model *GlobalKIN* was used. We first addressed the importance of NO^- and NO_2^- in the reaction mechanism and their effects on the densities of electrons, $O_2(^1\Delta)$ and $O_2(^1\Sigma)$. The densities of these species are shown along the axis of the discharge in figure 4 for a 3 Torr mixture of He/O_2/NO = 60/30/10 with 40 W power deposition. A high mole fraction of NO was used as an extreme case. When including NO^- and NO_2^- the peak electron density decreased approximately 10% from 1.4×10^{10} cm^{-3}. The reduction in n_e results in large part from the attachment of electrons to NO through 3-body reactions similar to those for O_2^- formation (equation (7)) and dissociative attachment to NO. The changes in densities of $O_2(^1\Delta)$ and $O_2(^1\Sigma)$ were relatively small (<5%) and could be attributed to the fact that n_e decreases and T_e increases modestly (0.05–0.1 eV from ≈2.0 eV) with the inclusion of NO^- and NO_2^-. (Recall that electron impact excitation of $O_2(^1\Delta)$ is maximum for T_e = 1–1.5 eV.) The density of O atoms was relatively independent on the inclusion of NO^- and NO_2^-. Based on these trends, we can expect results from *nonPDPSIM* (which do not include NO^- and NO_2^- in the reaction mechanism) to over-predict $O_2(^1\Delta)$ densities by a few per cent.

The consequences of NO in the inlet flow on the maximum densities of charged species, T_g, T_e, and power deposition into different species by electron impact are shown in figure 5 for 3 Torr and 40 W. A modest increase in n_e, from 1.1×10^{10} cm^{-3} to 1.25×10^{10} cm^{-3}, occurs as the NO mole fraction is increased from 0 to 10% due to the higher rates of ionization with NO in spite of a decrease in the positive and negative

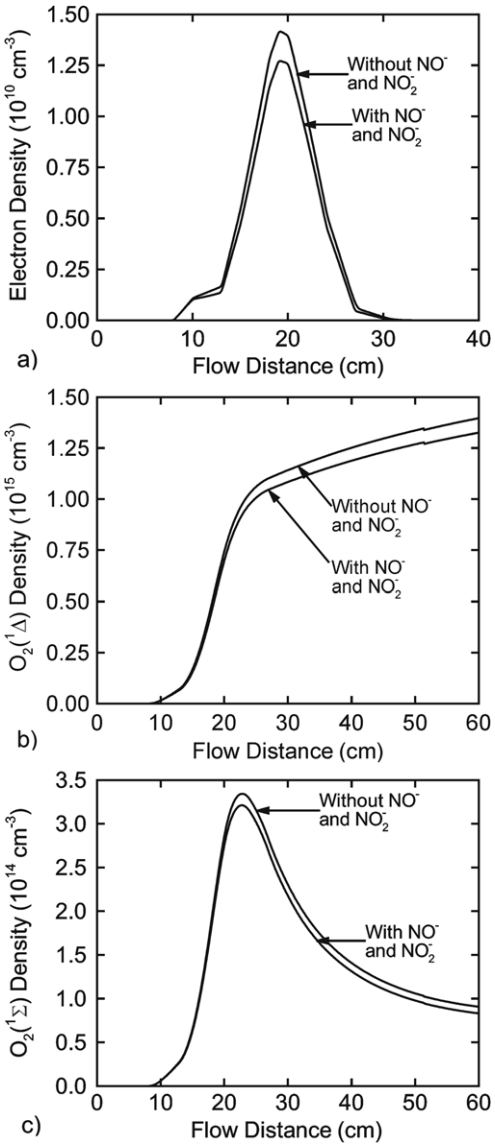

Figure 4. Dependence of plasma characteristics on the inclusion of NO^- and NO_2^- for 3 Torr, 40 W, He/O_2/NO = 60/30/10 and 6 slpm. Densities of (*a*) electrons, (*b*) $O_2(^1\Delta)$ and (*c*) $O_2(^1\Sigma)$. The densities of O did not show any noticeable variation. These results are from the plug flow model. Inclusion of these negative ions produces nominal changes in excited state densities.

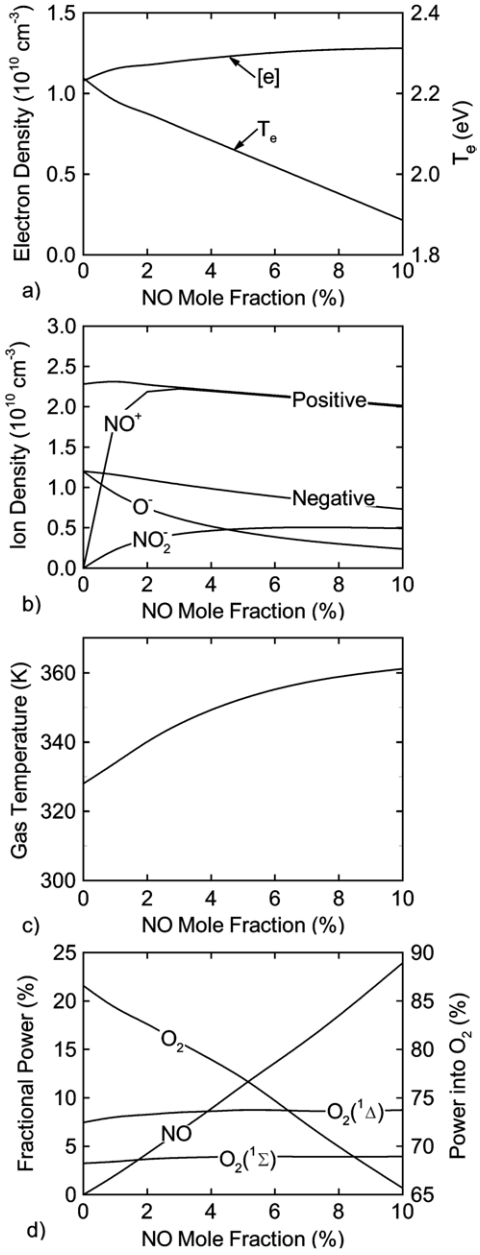

Figure 5. Plasma and gas characteristics while varying the NO mole fraction for 3 Torr, 40 W and a 6 slpm flow of He/O_2/NO = $70 - x/30/x$. (*a*) Maximum n_e, (*b*) maximum positive- and negative-ion densities, (*c*) maximum T_g and (*d*) fractional power deposition into O_2 and NO, and in producing $O_2(^1\Delta)$ and $O_2(^1\Sigma)$. These results are from the plug flow model and from calculations of EEDs. In spite of NO consuming a large fraction of the power, the decrease in T_e increases the rate of excitation of $O_2(^1\Delta)$ and so there is not a large change in power dissipated in exciting $O_2(^1\Delta)$.

ion densities. The increase in n_e results from the density of negative ions decreasing more rapidly than the positive ions when increasing the mole fraction of NO. The positive ion density decreases from 2.3×10^{10} cm^{-3} to 2.0×10^{10} cm^{-3} while the decrease in negative ion density is 1.2×10^{10} cm^{-3} to 0.75×10^{10} cm^{-3}. T_e decreases from 2.2 to 1.9 eV as the NO mole fraction is increased from 0 to 10%. The reduction in T_e is due to the additional power loss resulting from electron impact on NO when substituting NO for He and the reduction in the average ionization potential thereby enabling the discharge to be self-sustained with a lower value of T_e. This trend is partially offset by the additional attachment probability represented by NO.

While the total ion densities gradually decrease with increasing NO mole fraction, the densities of individual ions show more variation. In the absence of NO, O_2^+ forms the majority (>99%) of the positive ions. However with as little as 1–2% of NO, the majority ion is NO^+. This is due to charge exchange reactions between O_2^+ and NO. The dominant negative ion in the absence of NO is O^-, and as the NO mole fraction is increased, the density of NO_2^- ions increases, a result of charge exchange between O^- and NO_2 (equation (17)).

T_g increases with NO mole fraction primarily due to the exothermicity of reactions between O, NO and NO_2

(equations (18) and (19)). In the absence of NO, the maximum value of T_g is 328 K (increasing from the inlet value of 300 K). This value increases to 362 K with 10% NO. The peak gas temperatures occur just downstream of the discharge region. With large NO mole fractions, the contribution of Frank–Condon gas heating due to dissociation of NO can be more than a few per cent.

The fractional power deposited into NO increases nearly linearly with the NO mole fraction, increasing to 25% for an NO mole fraction of 10%. (Note that these values were computed using the actual mole fractions of species in the discharge and not the inlet conditions.) Correspondingly, the power deposition into O_2 decreases, from more than 85% in the absence of NO to 66% for an NO mole fraction of 10%. (Little power is dissipated by He.) In spite of the fraction of discharge power dissipated in O_2 decreasing, the power expended in exciting $O_2(^1\Delta)$, α, was relatively constant, reaching a shallow maximum of 8.7% for a NO mole fraction of 5%. As the NO mole fraction increases, T_e decreases from 2.2 to 1.9 eV thereby increasing the efficiency of $O_2(^1\Delta)$ production by electron impact [11]. Fortuitously, a combination of decreasing power dissipated by O_2 and an increase in the efficiency of exciting of $O_2(^1\Delta)$ maintains the total power expended in exciting $O_2(^1\Delta)$ relatively constant. This is not necessarily a general result but lowering T_e is generally beneficial. Similar trends are seen for $O_2(^1\Sigma)$ as the fractional power expended in exciting $O_2(^1\Sigma)$ increases slightly from 3.2% to 3.9% as the NO mole fraction increases to 10%.

The consequences of NO mole fraction in the inlet flow on the densities of O, $O_2(^1\Delta)$ and $O_2(^1\Sigma)$, and the yield of $O_2(^1\Delta)$ along the axis of the discharge are shown in figure 6 for the base case of 3 Torr, 40 W and 30% O_2. (Note that this yield is based on the mole fraction equivalent of O_2 for all oxygen species [11].) A flow of 100 sccm of He/I_2 = 99/1 is injected through the second nozzle. In the absence of NO, the density of $O_2(^1\Delta)$ increases to 1.2×10^{15} cm^{-3}due to electron impact excitation as the inlet flow passes through the plasma zone. The increase in the density of $O_2(^1\Delta)$ to 1.75×10^{15} cm^{-3} after the discharge zone results largely from quenching of a density of 0.4×10^{15} cm^{-3} of $O_2(^1\Sigma)$ by O atoms and excitation transfer from $O(^1D)$. The density of $O_2(^1\Delta)$ upstream of the I_2 injection point monotonically decreases with the addition of NO, from 1.75×10^{15} cm^{-3} without NO to 1.1×10^{15} cm^{-3} with 10% NO. A portion of this decrease results from an increase in the T_g when adding NO though the yield of $O_2(^1\Delta)$ also decreases from 5.9% when adding NO.

The production of $O_2(^1\Delta)$ is dominated by electron impact on O_2 and so is dependent on T_e and n_e. Since the power deposition producing $O_2(^1\Delta)$ is nearly constant, secondary processes must be responsible for the decrease in the yield of $O_2(^1\Delta)$ with increasing NO. One such secondary process is the production of $O_2(^1\Delta)$ by excitation transfer between $O(^1D)$ and O_2. The majority of $O(^1D)$ is produced by dissociative excitation of O_2 (equation (5)). Reactions of $O(^1D)$ with O_2 produces its excited states,

$$O(^1D) + O_2 \rightarrow O + O_2(^1\Sigma),$$
$$(k = 2.6 \times 10^{-11} \exp(67/T_g)\ \text{cm}^3\ \text{s}^{-1}), \quad (37)$$
$$O(^1D) + O_2 \rightarrow O + O_2(^1\Delta),$$
$$(k = 1.5 \times 10^{-12} \exp(67/T_g)\ \text{cm}^3\ \text{s}^{-1}). \quad (38)$$

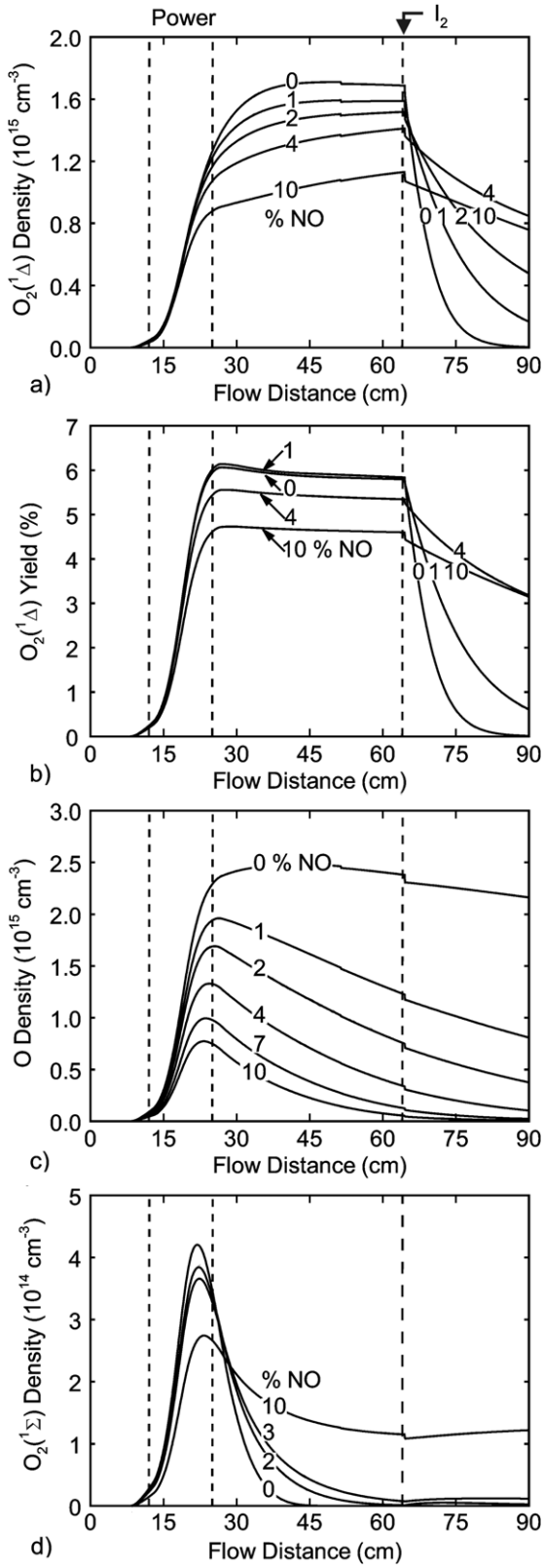

Figure 6. Densities of oxygen species and yield of $O_2(^1\Delta)$ along the axis of the tube while varying NO mole fraction for 3 Torr and 40 W for a 6 slpm flow of He/O_2/NO = $70 - x/30/x$. 100 sccm of He/I_2 = 99/1 is injected through the second nozzle. (*a*) $O_2(^1\Delta)$, (*b*) yield of $O_2(^1\Delta)$, (*c*) O and (*d*) $O_2(^1\Sigma)$. These results are from the plug flow model. Increasing flows of NO decrease the flow of O atoms.

With the decrease in T_e with addition of NO, the production of $O(^1D)$ by electron impact dissociation of O_2 decreases and so these secondary sources of $O_2(^1\Delta)$ and $O_2(^1\Sigma)$ also decrease. Furthermore, both NO and NO_2 are quenchers of $O(^1D)$,

$$NO + O(^1D) \rightarrow NO + O, \quad (k = 4.0 \times 10^{-11}\,cm^3\,s^{-1}), \tag{39}$$

$$NO_2 + O(^1D) \rightarrow NO + O_2, \quad (k = 3.0 \times 10^{-10}\,cm^3\,s^{-1}), \tag{40}$$

$$NO_2 + O(^1D) \rightarrow NO_2 + O, \quad (k = 3.2 \times 10^{-10}\,cm^3\,s^{-1}). \tag{41}$$

So the addition of NO reduces the production of $O(^1D)$ and increases its rate of quenching, thereby reducing the production of $O_2(^1\Delta)$ by excitation transfer. The importance of the quenching reactions of $O(^1D)$ is demonstrated by excluding the reactions in equations (39)–(41) from the mechanism. For 10% NO in the flow, the yield of $O_2(^1\Delta)$ improved from 4.6% to 5.3% when quenching of $O(^1D)$ is eliminated. The quenching of $O_2(^1\Delta)$ by NO has a small rate coefficient ($3.5 \times 10^{-17}\,cm^3\,s^{-1}$) and so does not significantly contribute to the loss of $O_2(^1\Delta)$.

The density of O atoms increases monotonically through the discharge zone to a maximum value of $2.5 \times 10^{15}\,cm^{-3}$ in the absence of NO. (The small increase in the density of O after the discharge is mainly due to gas cooling.) With the addition of NO, the density of O atoms decreases throughout the flow-tube and, in particular, downstream of the discharge. This decrease is due to both the reduction in the rate of electron impact dissociation of O_2 by the decrease in T_e and the formation of NO_2 in reactions with NO. In the post-discharge region in the absence of NO, the majority of $O_2(^1\Sigma)$ is converted to $O_2(^1\Delta)$ through collisions with O and O_3. Due to the reduction of O atoms with increasing NO, the rates of quenching of $O_2(^1\Sigma)$ to $O_2(^1\Delta)$ are also smaller, leading to higher densities of $O_2(^1\Sigma)$ in the afterglow. Higher $O_2(^1\Sigma)$ densities are not necessarily bad since they help in dissociating I_2 but maintaining those densities does result in lower densities of $O_2(^1\Delta)$ that directly pump I^*.

The densities of I and I^*, and the optical gain at 1.315 μ are shown in figure 7 for the conditions of figure 6 (1 sccm of I_2 injected in a 100 sccm, $He/I_2 = 99/1$ flow). The gain was given by $\sigma([I^*] - 0.5[I])$ where σ is the stimulated emission cross-section. At pressures of less than tens of Torr, Doppler broadening dominates over pressure broadening, and so the stimulated emission cross-section can be approximated by [35],

$$\sigma = 1.33 \times 10^{-16} T_g^{-1/2}\,cm^2. \tag{42}$$

In the absence of NO, the density of I increases from $1.75 \times 10^{13}\,cm^{-3}$ at the I_2 injection point to $3.2 \times 10^{13}\,cm^{-3}$ downstream due in large part to the reaction of O atoms with I_2. The density of I^* is maximum at the injection point at $1.45 \times 10^{13}\,cm^{-3}$ and decreases to negligible values by the end of the flow tube due to the depletion of $O_2(^1\Delta)$ (the species responsible for the pumping reaction) and quenching by O atoms. Since the lifetime of I^* (125 μs for quenching by O) is short compared with flow times, the density of I^* does not appreciably accumulate in the discharge and its density is a reflection of instantaneous production and quenching rates. The end result is a peak gain of $4.2 \times 10^{-5}\,cm^{-1}$ within a centimetre of the I_2 injection point. Note that the rate of quenching of I^* by O is faster than that due to spontaneous emission (0.1 s) [33].

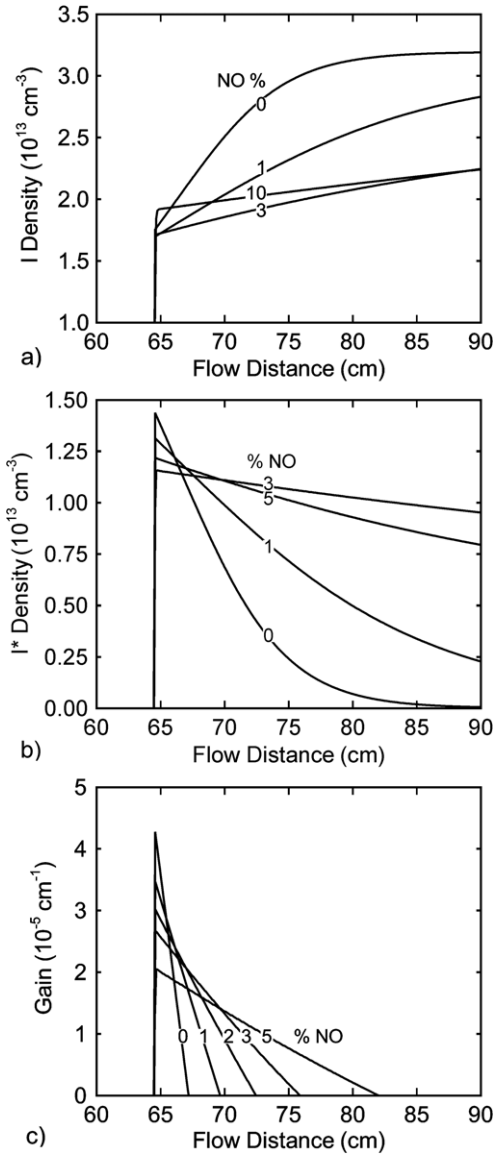

Figure 7. Densities of atomic iodine species as a function of inlet NO mole fraction for 3 Torr, 40 W, $He/O_2/NO = 70 - x/30/x$ and 6 slpm. 100 sccm of $He/I_2 = 99/1$ is injected through the second nozzle. Densities of (*a*) I, (*b*) I^* and (*c*) optical gain. These results are from the plug flow model. Low flows of NO produce the maximum peak gain whereas high flows of NO produce larger plumes of positive gain.

With injection of I_2 the density of $O_2(^1\Delta)$ decreases by virtue of excitation transfer and dissociative excitation of I_2, and reactions with I which pumps I^*. In the absence of NO, the density of $O_2(^1\Delta)$ is fully depleted by the reactions. In the absence of NO there is also a large density of O atoms at the injection point which react with I_2 producing IO and I. Since the rate of dissociation of I_2 by $O_2(^1\Delta)$ and $O_2(^1\Sigma)$ is slower than by O atoms there is a larger density of I available for $O_2(^1\Delta)$ to react with, and so the $O_2(^1\Delta)$ is rapidly depleted.

As the flow of NO is increased, the flow of O atoms decreases, resulting in a lower rate of dissociation of I_2 and fewer I atoms. With the lower density of I the reactivity of $O_2(^1\Delta)$ is lower; and so its density decreases less rapidly after injection of I_2.

The production of I^* results from reactions of $O_2(^1\Delta)$ with I while the quenching of I^* is largely due to collisions with O atoms. Increasing the NO mole fraction decreases the O atom density downstream thereby lowering the rates of quenching of I^* and extending its plume beyond the I_2 injection point. However, having too large an NO mole fraction results in too low rates of dissociation of I_2 and hence poor utilization of $O_2(^1\Delta)$. The end result is that the region over which positive gain can be sustained is maximum for an intermediate mole fraction of NO of 3%.

The purpose of flowing NO (or injecting NO_2) is largely to manage the O atom density and so control the quenching of I^* by O. A sensitivity study was conducted of the rate coefficient for this quenching reaction from the nominal value of 8×10^{-12} cm^3 s^{-1}. The densities of $O_2(^1\Delta)$ and I^*, and gain are shown in figure 8 while varying this rate coefficient from 0 to 1.0×10^{-11} cm^3 s^{-1}. In the absence of quenching, the densities of I^* and $O_2(^1\Delta)$ do not significantly decrease downstream of the I_2 injection point. In the absence of quenching by O, the predominant quencher of I^* is O_2 and this quenching produces $O_2(^1\Delta)$. The forward and backward pumping reactions (equations (25) and (26)) reach an equilibrium where the I^* and $O_2(^1\Delta)$ densities gradually decrease due to minor quenchers of I^* (such as NO and $O_2(^1\Delta)$) and radiative relaxation. When increasing the rate coefficient for quenching I^*, the density of I^* decreases proportionately. By removing I^* in this manner the rate of the backward reaction with O_2 decreases and so does the density of $O_2(^1\Delta)$. The extent of positive gain is progressively limited to the few cm beyond the I_2 injection point as the quenching of I^* increases, though the peak value of gain is not particularly sensitive to the rate coefficient.

The densities of $O_2(^1\Delta)$ and O, and T_g 2 cm upstream of the second nozzle are shown in figure 9 as a function of power deposition and NO mole fraction in the inlet flow. In general, T_g increases with power deposition and with NO addition reaching a maximum of 480 K with 400 W power deposition and 10% NO in the inlet flow. Increasing power deposition produces more electron impact dissociation of O_2 and NO, producing larger densities of O atoms. However, increasing NO mole fractions decreases the density of O atoms by virtue of scavenging by NO and NO_2 and decreasing T_e.

The density of $O_2(^1\Delta)$ decreases with NO addition, as discussed above, and increases with power deposition. The saturation in the density $O_2(^1\Delta)$ at 6.5×10^{15} cm^{-3} at higher powers is due in part to the depletion of O_2 by electron impact dissociation and in part to gas heating. For example, with 400 W and 0% NO, the fractional dissociation of O_2 is 68%. The addition of NO reduces the depletion of O_2 by both reducing the rate of O_2 dissociation and by recycling O atoms back to O_2. For example, for 10% NO addition and 400 W, the fractional dissociation decreases to 36%. The yield of $O_2(^1\Delta)$ saturates with power at 18% due to the depletion of O_2.

The densities of I and I^*, and gain as function of power deposition and NO mole fraction are shown in figure 10 at a location of 2 cm downstream from the I_2 injection point. This mixing length of 2 cm was chosen based on previous studies

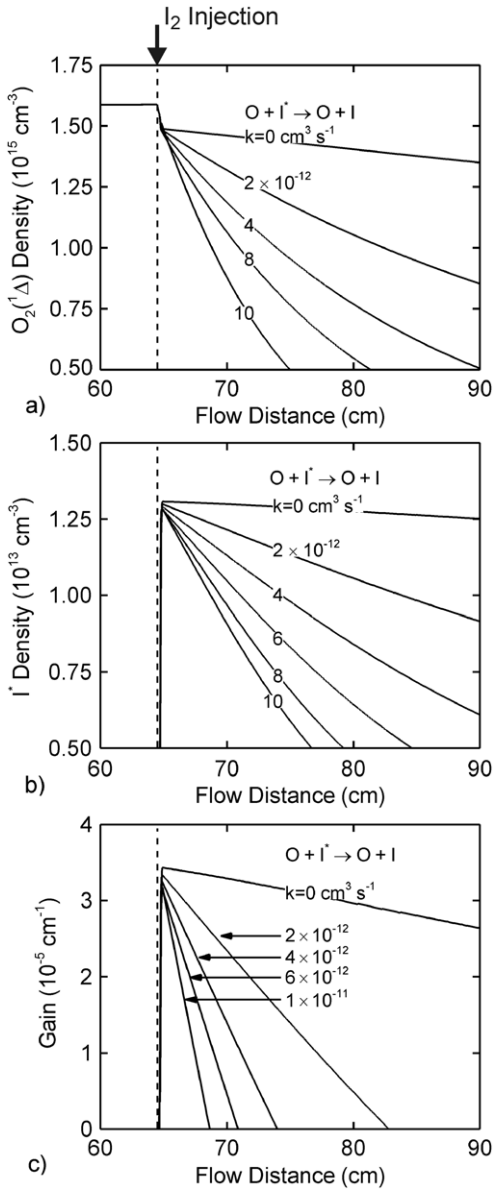

Figure 8. Sensitivities of the value of the rate coefficient for the quenching reaction between O and I^* on the post-discharge kinetics for 3 Torr, 40 W, He/O_2/NO = 69/30/1 and 6 slpm. 100 sccm of He/I_2 = 99/1 is injected through the second nozzle. Densities of (*a*) $O_2(^1\Delta)$, (*b*) I^* and (*c*) optical gain. These results are from the plug flow model.

for similar flow conditions [36]. The inlet flow has 30% O_2 and the flow injected through the second nozzle is 1 sccm of I_2 in a 100 sccm flow of He/I_2 = 99/1. At low power deposition, the density of I is large, $(2.2–2.3) \times 10^{13}$ cm^{-3}, because the yields of $O_2(^1\Delta)$ are low enough that the pumping of I to I^* is slow. As the yield of $O_2(^1\Delta)$ increases at higher powers, the pumping reactions reduce the density of I and increase that of I^*, leading to an increase in gain. However, at large power deposition, the density of O increases whereas that of $O_2(^1\Delta)$ saturates. This leads to an increased rate of quenching of I^* by O which reduces the density of I^* and increases that of I. The end result is a reduction in gain.

Increasing NO in the inlet flow reduces the density of O atoms at the injection point, thereby reducing the rate of

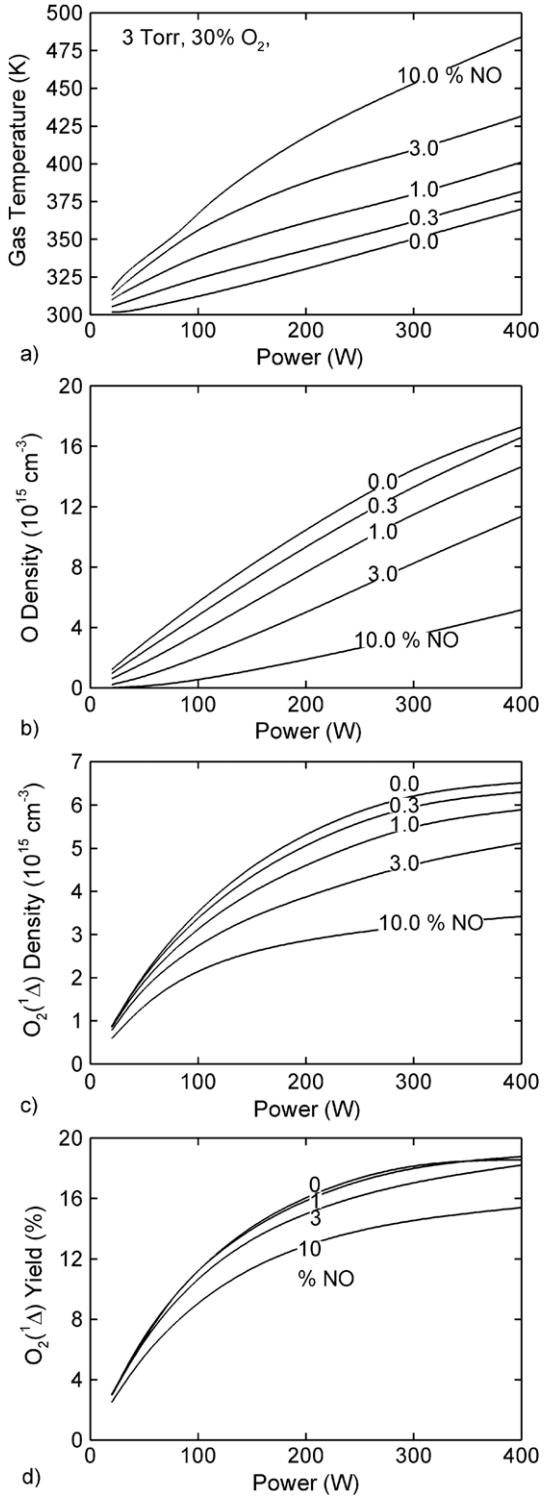

Figure 9. Consequences of power deposition and NO mole fraction on the neutral gas properties for 3 Torr, $He/O_2/NO = 70 - x/30/x$ and 6 slpm. (*a*) T_g, (*b*) density of O, (*c*) density of $O_2(^1\Delta)$ and (*d*) yield of $O_2(^1\Delta)$. $O_2(^1\Delta)$ densities saturate with power due to a high degree of dissociation of O_2. These results are from the plug flow model and the values are for 2 cm upstream of the second nozzle.

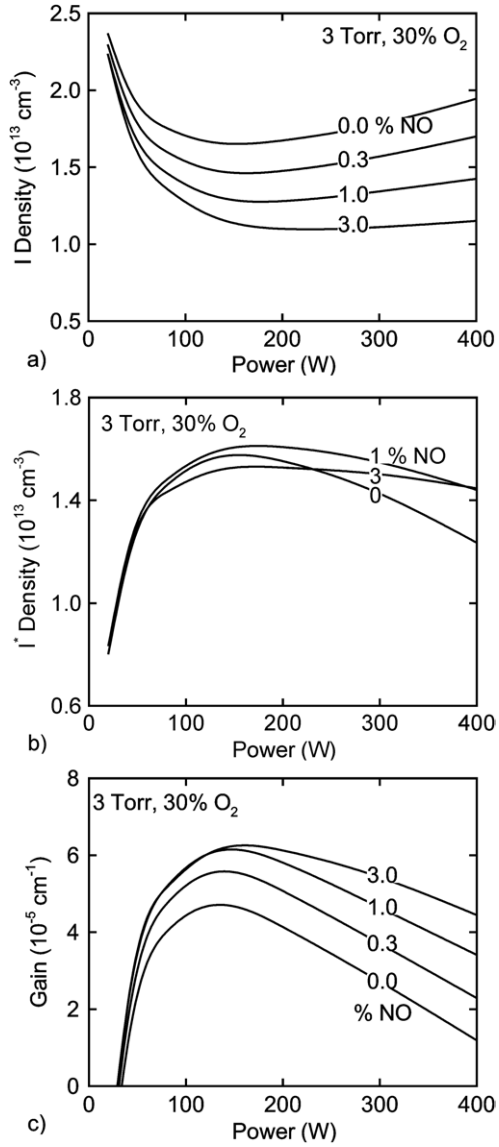

Figure 10. Consequences of power deposition and NO mole fraction on iodine species and gain for 3 Torr, $He/O_2/NO = 70 - x/30/x$ and 6 slpm. Densities of (*a*) I and (*b*) I^* and (*c*) optical gain. These results are from the plug flow model and the values are for 2 cm downstream of the second nozzle. Gain is maximum at high power only with high flow rates of NO.

dissociation of I_2 and the density of I atoms. The reduction in O by addition of NO also reduces the quenching of I^* by O, making the gain predominantly dependent on the yield of $O_2(^1\Delta)$. As a result, for 3% NO, the gain decreases from 6.0 $\times 10^{-5}$ to 4.3 $\times 10^{-5}$ cm^{-1} between 150 and 400 W, whereas in the absence of NO, the gain reduces by nearly a factor of 3.

The eCOIL system may operate in either power limited or iodine limited modes. In the iodine limited mode, the flow of $O_2(^1\Delta)$ and O generated by the discharge fully utilizes the injected flow of I_2, and so gain saturates with increasing power. To some degree (quenching of I^* and depletion of O_2 aside), this is the mode that applies to the results shown in figure 10. In the power limited mode, the flow of $O_2(^1\Delta)$ and O is insufficient to fully utilize the injected flow of I_2, and so gain saturates with flow of I_2.

These modes of operation are demonstrated by varying power deposition and I_2 flow rate. The densities of I and I^*, and gain are shown 2 cm downstream of the I_2 injection point in figure 11 for a 6 slpm inlet flow of $He/O_2/NO = 67/30/3$

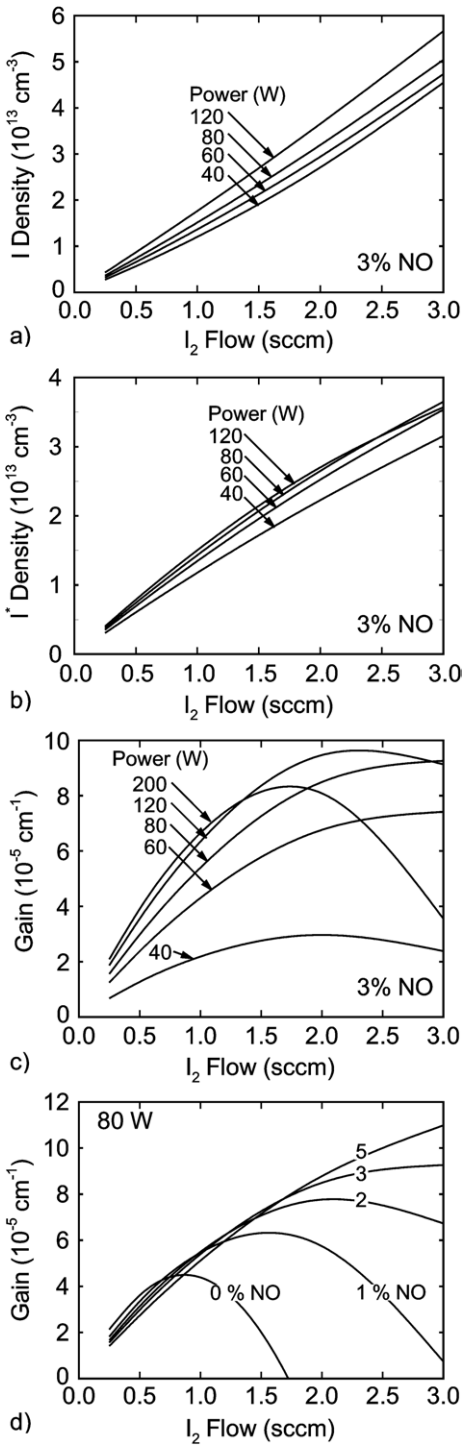

Figure 11. Iodine species densities and gain while varying the I_2 flow rate through the second nozzle. Densities of (*a*) I and (*b*) I*, and (*c*) optical gain for 3% NO in the inlet flow and (*d*) gain for 80 W power deposition. These results are from the plug flow model and the values are for 2 cm downstream of the second nozzle. Varying power and I_2 flow rate switches between the power limited and I_2 limited regimes.

while varying power and I_2 flow rate. The densities of I and I* increase nearly linearly with the flow of I_2 and increase sub-linearly with power deposition. For example, with a flow of 3 sccm of I_2, the density of I is 4.6×10^{13} cm^{-3} with 40 W and only 5.6×10^{13} cm^{-3} with 120 W. For these conditions the production of I is limited by the availability of I_2 as the injected I_2 is nearly completly dissociated by reactions with O, $O_2(^1\Delta)$ and $O_2(^1\Sigma)$ for all power depositions. The production of I* is limited by the yield of $O_2(^1\Delta)$ which does not scale linearly with power at higher power depositions. As a consequence the density of I* saturates with power deposition with large flows of I_2. This saturation is exacerbated at high power depositions (or low NO mole fractions) by large densities of O which quench I*.

With a power deposition of 40 W, gain increases with flow rate of I_2 (shown in figure 11(*c*)) saturating at 3×10^{-5} cm^{-1} at 2 sccm, a consequence of being in a power limited regime. As the power increases the gain increases, and the I_2 flow rate at which the maximum gain is obtained also increases. For example, for 80 W, the gain saturates at 9×10^{-5} cm^{-1} for an I_2 flow rate of 3 sccm. The higher power deposition is able to better utilize the increased flow of I_2. As the power further increases, the peak gain increases only moderately and decreases above 200 W as the system transitions to an I_2 limited regime and the densities of $O_2(^1\Delta)$ saturate.

The consequences of flow rates of NO and I_2 on gain are shown for 80 W in figure 11(*d*). For a fixed power, increasing the mole fraction of NO at the inlet reduces the density of O atoms which reduces the quenching of I*. Increasing the NO mole fraction increases the range of I_2 flow rates over which the positive gain can be achieved and increases the flow rate of I_2 at which the maximum gain is obtained. For example, the maximum gain in the absence of NO is 4.2×10^{-5} cm^{-1} for an I_2 flow rate of 0.8 sccm. As the rate of quenching of I* decreases with increasing NO flow, gain increases to more than 1.2×10^{-4} cm^{-1} for an inlet mole fraction of 5% NO and flow rate of 3 sccm of I_2.

The consequences of flow dynamics on the densities of $O_2(^1\Delta)$ and I* are shown in figure 12 with results from *nonPDPSIM*. The densities of $O_2(^1\Delta)$ and I* are shown for 80 W and a 6 slpm inlet flow of He/O_2/NO = 68/30/2. A 100 sccm flow of He/I_2 was injected from the second nozzle with the I_2 flow varied from 0.5 to 3 sccm. As the flow passes through the discharge zone, electron impact produces $O_2(^1\Delta)$ at large radius first where the plasma density is highest. Diffusion homogenizes the density of 2.5×10^{15} cm^{-3} across the radius by 10–12 cm downstream of the plasma zone. At and after the I_2 injection point, the densities of $O_2(^1\Delta)$ decrease due to excitation transfer to I_2 and pumping of I*, first at the outer radius where the I_2 is injected and on axis 4–5 cm downstream. With low flow rates of I_2 ($\leqslant$0.5 sccm), the $O_2(^1\Delta)$ is not significantly depleted whereas with flow rates $\geqslant$1 sccm, the flow of $O_2(^1\Delta)$ is largely consumed by reactions with I_2 and I.

The densities of I* are maximum adjacent to the second nozzle where densities of both $O_2(^1\Delta)$ and I_2 are largest. The I* diffuses radially to the centre of the discharge 4–5 cm downstream of the injection point. For small flow rates of I_2, the densities of I are smaller, and hence consumption of $O_2(^1\Delta)$ in pumping the I* is gradual, leading to a longer distance over which significant amounts of I* are present. At high flow rates of I_2, $O_2(^1\Delta)$ is largely consumed in the vicinity of the injection point and so I* does not extend appreciably beyond that point.

The densities of I and I*, and the gain obtained with *nonPDPSIM* at a radius of 1.5 cm are shown in figure 13 for

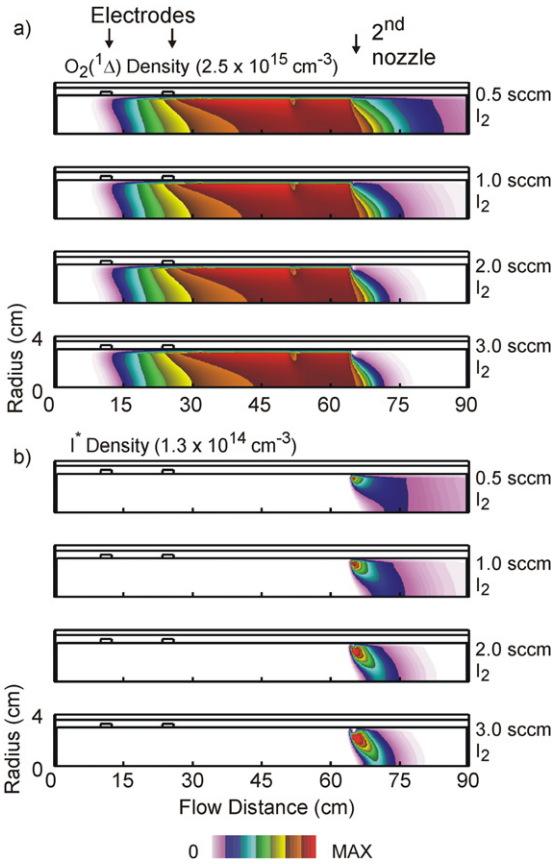

Figure 12. Excited state densities while varying the I_2 flow rate through the second nozzle. (*a*) $O_2(^1\Delta)$ and (*b*) I^*. These results, obtained with *nonPDPSIM*, are for 3 Torr, 80 W power deposition, and 6 slpm flow of $He/O_2/NO = 68/30/2$.

the conditions of figure 12. Similar to the results obtained with *GlobalKIN*, the densities of I increase with increasing flow rate of I_2 indicating that the system is in an I_2 limited regime. The densities of I^* also increase with increasing I_2 mole fraction reaching a maximum 3–4 cm downstream of the injection point. I^* is rapidly quenched by the O atoms whose densities are commensurate with $O_2(^1\Delta)$. At lower I_2 mole fractions, the densities of I^* do not decrease rapidly downstream of the injection point due to the availability of $O_2(^1\Delta)$ to continue to pump I to I^*.

The maximum gain (at a radius of 1.5 cm) is 10^{-4} cm^{-1} for an I_2 flow of 3 sccm. The axial extent of positive gain is limited by the depletion of $O_2(^1\Delta)$. Lower flow rates of I_2 produce lower gain but the axial extent of gain is greater. A comparison of maximum gain obtained with *GlobalKIN* and *nonPDPSIM* as a function of flow rate of I_2 is shown in figure 13(*d*). The predicted gains are commensurate except at large flow rates of I_2 where the gain with *GlobalKIN* is significantly higher than with the 2d model. The lack of axial transport in the plug flow model produces artificially high rates of reaction between O and $O_2(^1\Delta)$ with I and I_2, which increases predicted gain.

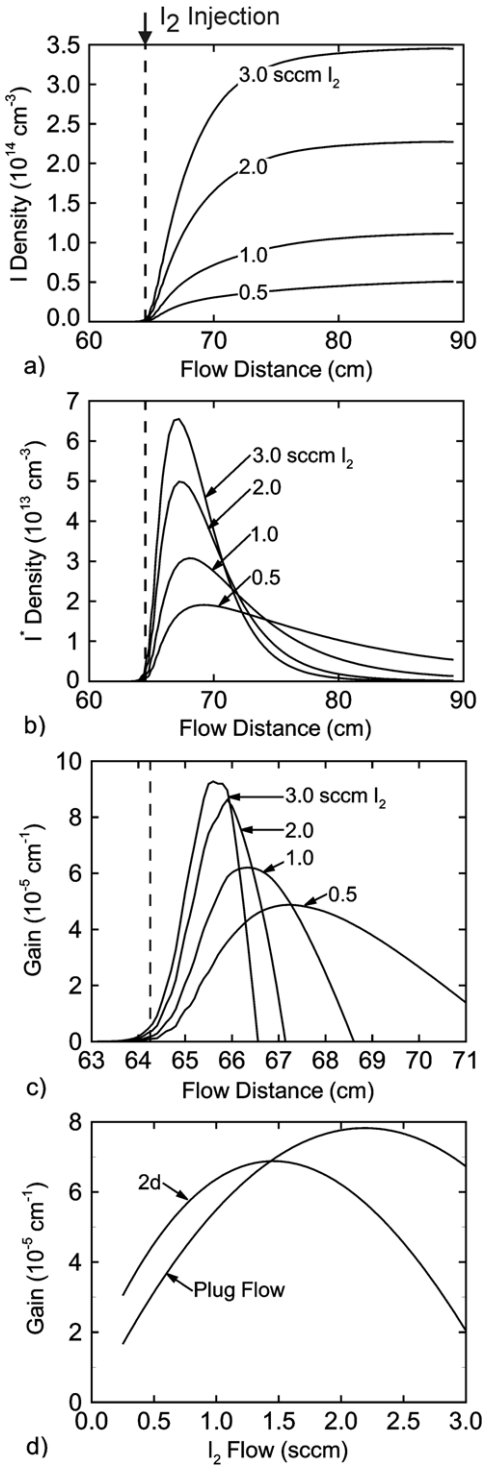

Figure 13. Iodine species densities and gain at a radius of 1.5 cm as a function of the flow rate of I_2 through the second nozzle. Densities of (*a*) I and (*b*) I^*, (*c*) gain and (*d*) comparison of the plug flow and 2D models for gain 2 cm downstream of the second nozzle. These results are from *nonPDPSIM* for 3 Torr, 80 W power deposition and 6 slpm flow of $He/O_2/NO = 68/30/2$. 100 sccm of He/I_2 is flowed through the second nozzle.

5. NO_2 injection

In experimental demonstrations of laser oscillation and significant gain in eCOIL systems, NO_2 was usually injected downstream of the plasma zone and prior to the addition of I_2 [9, 34]. Comparisons between predictions from *GlobalKIN* and experiments by Carroll *et al* [34] using this strategy are shown in figure 14. The conditions are a 10 Torr, 26.9 slpm

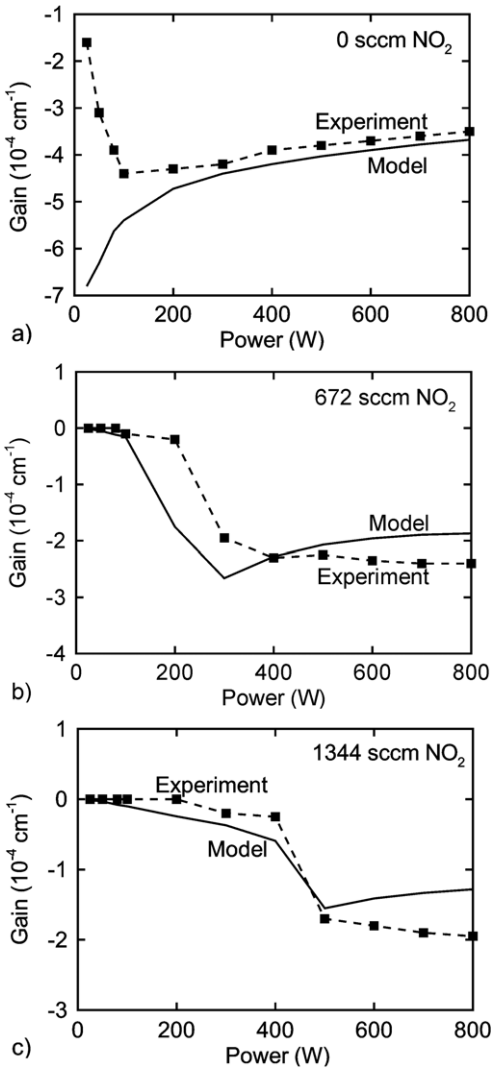

Figure 14. Gain in a subsonic flow for 10 Torr, 26.9 slpm of $He/O_2 = 80/20$, 25–800 W, with 10.8 sccm of I_2 injected through the second nozzle. (a) 0 sccm NO_2, (*b*) 672 sccm NO_2 and (*c*) 1344 sccm NO_2 through the first nozzle. Experimental values are from [34].

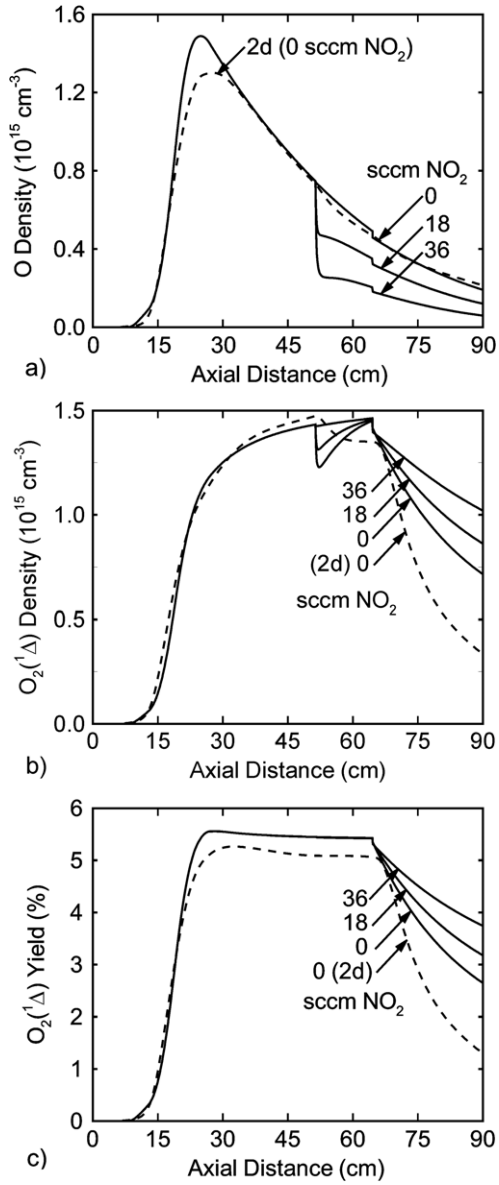

Figure 15. Consequences of injection of NO_2 through the first nozzle for 3 Torr, 40 W, $He/O_2/NO = 67/30/3$ and 6 slpm. 36 sccm of He/NO_2 mixture is injected through the first nozzle. Densities of (*a*) O and (*b*) $O_2(^1\Delta)$ and (*c*) yield of $O_2(^1\Delta)$. Addition of NO_2 rapidly consumes the O atoms. These results are from the *GlobalKIN*, the plug flow model. Values from the 2D *nonPDPSIM* are shown without NO_2 injection.

(20 mmol s^{-1}) inlet flow of $He/O_2 = 80/20$ and 25–800 W followed by injection of 0–1344 sccm (0–1 mmol s^{-1}) NO_2 and injection of 10.7 sccm (0.008 mmol s^{-1}) of I_2, equivalent to few per cent of the $O_2(^1\Delta)$ flow rate. The diameter of the reactor is 4.9 cm and I_2 injection is 20 cm downstream of the NO_2 injection point. The power deposition spans nearly 25 cm due to a larger separation between electrodes in the experiment. The experimental measurements were made 10 cm downstream of the I_2 injection point in a subsonic (high gas temperature flow) and so gains are negative.

With the exception of low powers and low flow rates of NO_2, the experimental trends are captured by *GlobalKIN*. Addition of NO_2 prior to injection of I_2 scavenges some of the O atoms in the flow and so reduces the quenching of I^* by O atoms. Higher powers produce larger flows of O atoms as well as more $O_2(^1\Delta)$ but the quenching of I^* dominates. Increasing the NO_2 flow rate increases the scavenging of O atoms and extends the power prior to transitioning to large negative gain.

Since NO_2 is more effective than NO in scavenging of O atoms, we investigated NO_2 injection through the first nozzle. The conditions are a 3 Torr, 6 slpm inlet flow of $He/O_2/NO = 67/30/3$ and discharge power of 40 W. A He/NO_2 flow of 36 sccm was injected through the first nozzle with the fraction of NO_2 being varied. As before a 100 sccm flow of $He/I_2 = 99/1$ was injected through the second nozzle.

The consequences of NO_2 flow rate through the first nozzle on the densities of O and $O_2(^1\Delta)$, and yield of $O_2(^1\Delta)$ are shown in figure 15. These results are from *GlobalKIN* with a result from *nonPDPSIM* without NO_2 injection for comparison. The injection of NO_2 produces a decrease in the O atom density due to the titration of O by NO_2 and the

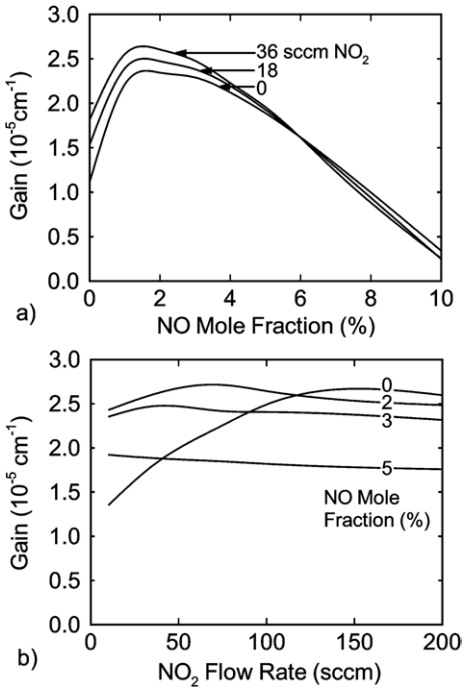

Figure 16. Gain when including NO in the inlet flow and injecting NO_2 through the first nozzle for 3 Torr, 40 W, $He/O_2/NO = 70 - x/30/x$ and 6 slpm. 100 sccm of $He/I_2 = 99/1$ is injected through the second nozzle. (*a*) Gain as a function of NO mole fraction and (*b*) gain as a function of NO_2 flow rate. These results are from the plug flow model. Maximum gain is obtained at low NO flow rates and high NO_2 injection.

conversion of O to O_2, respectively. As the NO_2 flow rate increases to 36 sccm the O atom densities decrease by a factor of 3–4 just downstream of the injection point due to the more rapid rate of reaction with O (compared with that of NO). The heat of reaction between NO_2 and O locally increases the gas temperature leading to a reduction in the density of $O_2(^1\Delta)$ near the first nozzle due to rarefaction. Note, however, that the yield of $O_2(^1\Delta)$ is not affected by NO_2 injection because NO_2 does not appreciably quench $O_2(^1\Delta)$. The reduction in the densities of O with NO_2 injection implies that the quenching of I^* by O is reduced. This produces a reduction in the amount of $O_2(^1\Delta)$ used in pumping the I^*. Hence, downstream of the second nozzle, the yield of $O_2(^1\Delta)$ is higher for larger NO_2 mole fractions. Results from *GlobalKIN* and *nonPDPSIM* are in general agreement except downstream of the I_2 injection point due to the artificially higher rates of reaction upon injection of I_2.

Gain is shown in figure 16 for 2 cm downstream from the second nozzle as a function of NO mole fraction in the inlet flow and flow rate of NO_2 through the second nozzle. The flow conditions are 3 Torr and 40 W power deposition. Having NO in the inlet flow affects the production of $O_2(^1\Delta)$ as discussed above as well as managing the O atoms density. Injection of NO_2 downstream of the discharge largely only affects the density of O atoms (and gas temperature). As such, at low values of NO flow, injection of NO_2 is effective in managing the O atom density and larger flow rates tend to maximize gain by reducing quenching of I^* by O atoms. At large flow rates of NO, the management of O atoms is dominated by reactions with NO, and so the injection of NO_2 is less effective. Since there is a deleterious effect on $O_2(^1\Delta)$ production by having large flows of NO through the discharge, managing the O atom density with injection of NO_2 is likely the optimum strategy.

6. Concluding remarks

The consequences of NO in the inlet flow of a He/O_2 plasma and its flowing afterglow, and NO_2 and I_2 injection on the post-discharge kinetics of the eCOIL were investigated using plug flow and 2D models. The addition of NO to the inlet flow through the discharge produces a reduction in T_e and a modest increase in n_e resulting in the densities and yields of $O_2(^1\Delta)$ being generally lower with NO. Including NO in the flow reduces the density of O atoms both by a reduction in the electron impact dissociation of O_2 and by exothermic reactions of O with NO. This proves beneficial to improving optical gain by reducing the quenching of I^* by O atoms. At higher power deposition, the dissociation of O_2 saturates the yield of $O_2(^1\Delta)$. By virtue of adding NO to the inlet flow, the reduction in T_e reduces the rate of dissociation of O_2. Even though the yields of $O_2(^1\Delta)$ were generally lower, the optical gain was generally higher when the NO mole inlet mole fraction was between 1% and 3%.

The eCOIL system can operate in power limited and I_2 limited regimes. At low flow rates, I_2 is nearly totally dissociated and so the densities of I depend largely on the I_2 flow rate. Upon increasing the flow rate of I_2, the system transitions to a power limited regime and higher powers are required to optimize gain. Small flows of NO_2 in the post-discharge region can be used to fine tune the gain. The addition of NO_2 rapidly consumes O atoms without significantly changing other parameters (other than T_g) and so increases the optical gain. The injection of NO_2 was most effective at low flow rates of NO. In general, management of the O atom density is critical to optimizing gain due to its rapid rate of quenching of I^*.

Acknowledgment

This work was supported by the Air Force Office of Scientific Research and the National Science Foundation (CTS-0520368).

References

[1] Hicks A, Utkin Yu G, Lempert W R, Rich J W and Adamovich I V 2006 *Appl. Phys. Lett.* **89** 241131
[2] Braginsky O V *et al* 2006 *J. Phys. D: Appl. Phys.* **39** 5183
[3] Verdeyen J T *et al* 2006 *Appl. Phys. Lett.* **89** 101115
[4] Kodymová J and Spalek O 1998 *Japan. J. Appl. Phys.* **37** 117
[5] Fujii H, Yoshida S, Iizuka M and Atsuta T 1990 *J. Appl. Phys.* **67** 3948
[6] Hill A 2000 The next generation of controlled avalanche discharge gas lasers *Int. Conf. on Lasers (Albuquerque, NM)*
[7] Hicks A *et al* 2005 *J. Phys. D: Appl. Phys.* **38** 3812
[8] Ionin A A *et al* 2003 *J. Phys. D: Appl. Phys.* **36** 982
[9] Palla A D, Carroll D L, Verdeyen J T and Solomon W C 2006 Effects of mixing on post-discharge modeling of ElectricOIL experiments *Proc. SPIE.* **6101** 610125
[10] Vasiljeva A N *et al* 2004 *J. Phys. D: Appl. Phys.* **37** 2455
[11] Stafford D S and Kushner M J 2005 *J. Appl. Phys.* **98** 073303
[12] Cook T J and Miller T A 1974 *Chem. Phys. Lett.* **25** 396

[13] Atkinson R *et al* 2000 *J. Phys. Chem. Ref. Data* **29** 167
[14] Stafford D S and Kushner M J 2004 *J. Appl. Phys.* **96** 2451
[15] Lay B, Moss R S, Rauf S and Kushner M J 2003 *Plasma Sources Sci. Technol.* **12** 8
[16] Kushner M J 2004 *J. Appl. Phys.* **95** 846
[17] Hon J *et al* 1994 *A Heuristic Method for Evaluating COIL Performance* AIAA Paper 94-2422
[18] Rapp D and Briglia D D 1965 *J. Chem. Phys.* **43** 1480
[19] Josic L, Wroblewski T, Petrovic Z Lj, Mechlinska-Drewko J and Karwasz G P 2001 *Chem. Phys. Lett.* **350** 318
[20] Lindsay B G, Mangan M A, Straub H C and Stebbings R F 2000 *J. Chem. Phys.* **112** 9404
[21] Vejby-Christensen L, Kella D, Pedersen H B and Andersen L H 1998 *Phys. Rev.* A **57** 3627
[22] Shimamori H and Hotta H 1988 *J. Chem. Phys.* **89** 2938
[23] Ikezoe Y, Matsuoka S, Takebe M and Viggiano A 1987 *Gas Phase Ion-Molecule Reaction Rate Constants Through 1986* (Ion Reaction Research Group of the Mass Spectroscopy Society of Japan, Tokyo, Japan)
[24] Atkinson R *et al* 2004 *Atmos. Chem. Phys.* **4** 1461
[25] Boodaghians R B, Borrell P M and Borrell P 1983 *Chem. Phys. Lett.* **97** 193
[26] Blais N C 1985 *J. Phys. Chem.* **89** 4156
[27] Doroshenko V M, Kudryavtsev V M and Smetanin V V 1992 *High Energy Chem.* **26** 227
[28] Gauthier M J E and Snelling D R 1975 *J. Photochem.* **4** 27
[29] Valli G S, Orru R, Clementi E, Lagana A and Crocchianti S 1995 *J. Chem. Phys.* **102** 2825
[30] Phillips L F and Schiff H I 1965 *J. Chem. Phys.* **42** 3171
[31] Campbell I M and Gray C N 1973 *Chem. Phys. Lett.* **18** 607
[32] Holscher D and Zellner R 2002 *Phys. Chem. Chem. Phys.* **4** 1839
[33] Husain D, Slater N K H and Weisenfeld J R 1977 *Chem. Phys. Lett.* **51** 201
[34] Carroll D L *et al* 2005 *IEEE J. Quantum Electron.* **41** 213
[35] Zagidullin M V, Nikolaev V D, Svistun M I, Khvatov N I and Hager G D 2005 *Appl. Phys. A: Mater. Process.* **81** 311
[36] Muruganandam T M *et al* 2002 *AIAA J.* **40** 1388